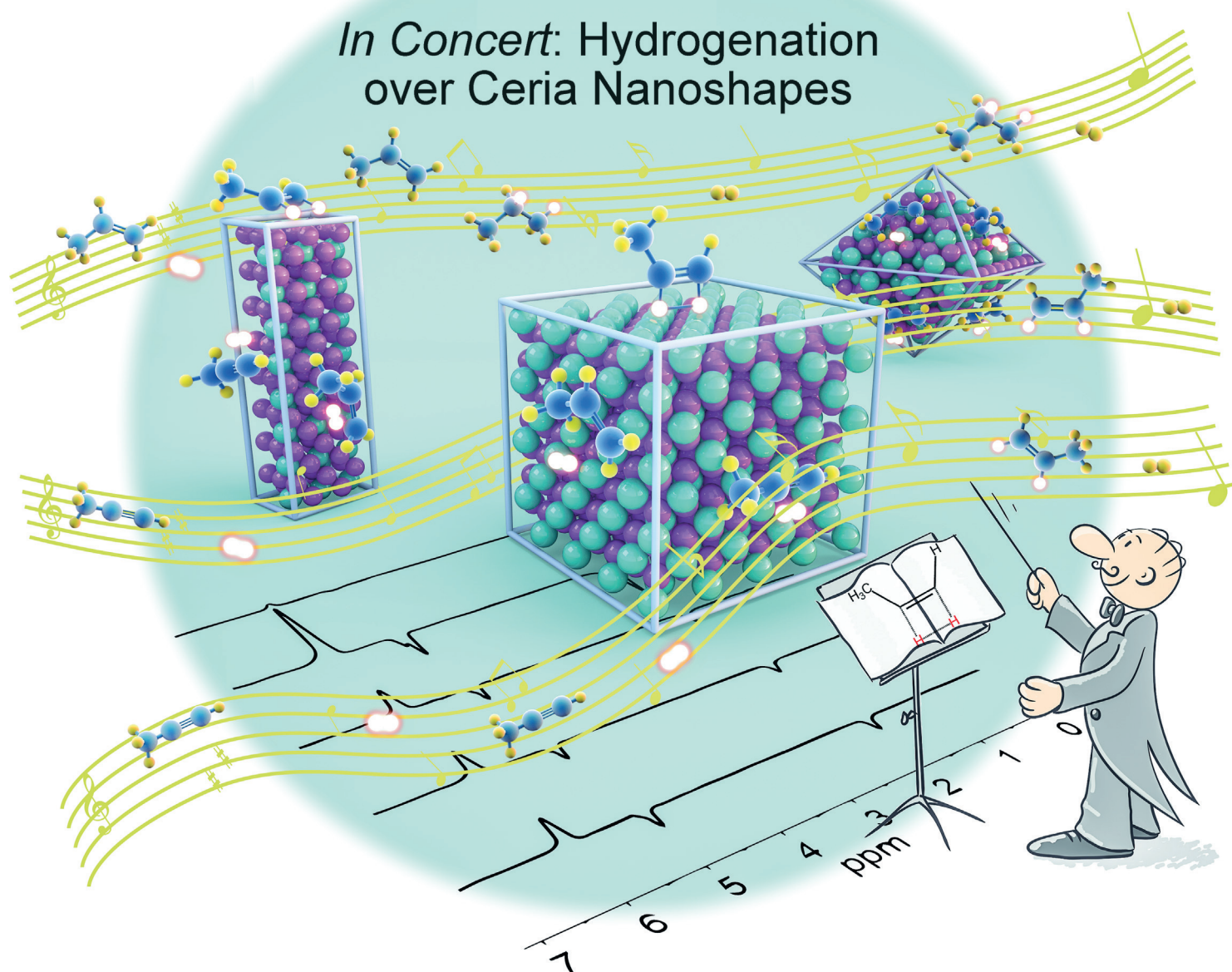# Shaped Ceria Nanocrystals Catalyze Efficient and Selective Para-Hydrogen-Enhanced Polarization

Evan W. Zhao, Haibin Zheng, Ronghui Zhou, Helena E. Hagelin-Weaver,* and Clifford R. Bowers*
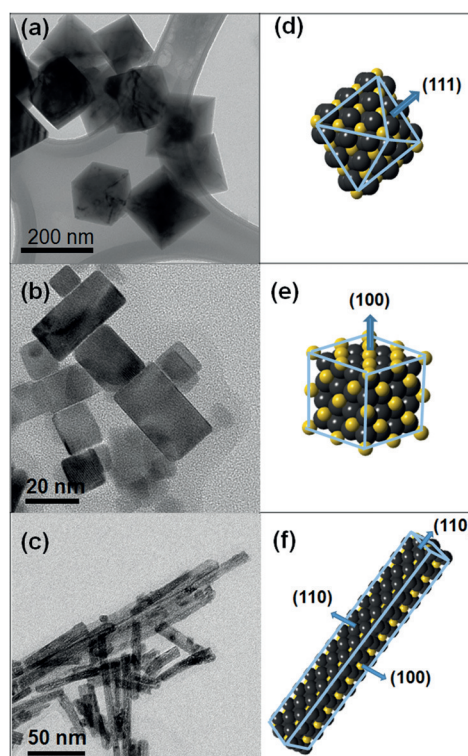
In Concert: Hydrogenation over Ceria Nanoshapes

Abstract: Intense para-hydrogen-enhanced NMR signals are observed in the hydrogenation of propene and propyne over ceria nanocubes, nano-octahedra, and nanorods. The well-defined ceria shapes, synthesized by a hydrothermal method, expose different crystalline facets with various oxygen vacancy densities, which are known to play a role in hydrogenation and oxidation catalysis. While the catalytic activity of the hydrogenation of propene over ceria is strongly facet-dependent, the pairwise selectivity is low (2.4% at 375°C), which is consistent with stepwise H atom transfer, and it is the same for all three nanocrystal shapes. Selective semi-hydrogenation of propyne over ceria nanocubes yields hyperpolarized propene with a similar pairwise selectivity of (2.7% at 300°C), indicating product formation predominantly by a non-pairwise addition. Ceria is also shown to be an efficient pairwise replacement catalyst for propene.

Para-hydrogen-induced polarization (PHIP)[1–6] is an inexpensive and scalable method for the bulk production of nuclear-spin-hyperpolarized fluids for NMR spectroscopy and imaging. Spin polarization of order unity is attainable but only if H_2 is added to the substrate in a pairwise fashion. PHIP NMR spectroscopy has been employed to study mechanisms of both homogeneous and heterogeneous hydrogenation catalysis.[7–10] Recent innovations have broadened the applicability of the technique.[11–19] Impurity-free hyperpolarized gases and liquids, with potential biomedical applications, can be prepared using supported metals and metal oxide catalysts (hetPHIP).[20–27] However, the reported low pairwise addition selectivity and limited generality remain as major obstacles to further development of the hetPHIP method.

Herein, a para-hydrogen-enhanced NMR study of the hydrogenation of propene (PE) and propyne (PY) over CeO_2 nanocrystals with three different shapes (Figure 1) is presented. Ceria has been the subject of numerous catalytic studies. The metal oxide is a highly active and selective catalyst of the hydrogenation of alkynes to alkenes,[28–33] and the activity with respect to PE hydrogenation is highly dependent on the CeO_2 surface structure.[31] Hyperpolarized alkenes produced by selective semi-hydrogenation can serve as precursors for the synthesis of other hyperpolarized species.[34]

Well-defined shapes are useful in catalysis studies as they facilitate investigations of the surface structure sensitivity.[35] Nanorods are terminated predominantly by (100) and (110) facets,[36] nanocubes by (100) facets, and octahedra by (111)

[*] E. W. Zhao, Dr. R. Zhou, Prof. C. R. Bowers
    Department of Chemistry, University of Florida
    Gainesville, FL 32611 (USA)
    E-mail: bowers@chem.ufl.edu

    H. Zheng, Prof. H. E. Hagelin-Weaver
    Department of Chemical Engineering
    University of Florida
    Gainesville, FL 32611 (USA)
   E-mail: hweaver@che.ufl.edu

    Supporting information for this article is available on the WWW under http://dx.doi.org/10.1002/anie.201506045.

Figure 1. TEM images of CeO₂ a) nano-octahedra, b) nanocubes, and c) nanorods. Structural models of a CeO₂ d) nano-octahedron, e) nanocube, and f) nanorod simulated by CrystalMaker.

terraces (see Figure 1 d–f). The synthesis of nanocrystals with these three shapes allows for investigations of the facet dependence of the pairwise addition and replacement processes. Polycrystalline CeO_2 nanoparticles, which expose mainly (111) terraces, are significantly more active than CeO_2 nanocubes with (100) surfaces.[31] This is attributed to differences in the oxygen vacancy densities on the various CeO_2 facets. High-energy CeO_2 (100) and (110) surfaces (rods and cubes) have more oxygen vacancies, which promote oxidation reactions, whereas low-energy, low-vacancy (111) surfaces favor hydrogenation.

Ceria is one of several polycrystalline metal oxides that have been reported to yield PHIP signals when PE is used as the substrate, although a temperature of 600°C was apparently required.[25] Kovtunov et al. briefly mentioned a PHIP effect for ceria, but did not include any PHIP spectra in their report, and the hydrogenation of PY was not studied with this catalyst. An investigation of PE and PY hydrogenation over CeO_2 nanocrystals with well-defined surface facets using PHIP NMR has never been reported.

In a recent DFT study, the hydrogenation of PE and PY over a CeO_2(111) surface was investigated.[33] The high selectivity of the semi-hydrogenation of PY to PE was explained by the exothermic adsorption of PY and endothermic adsorption of PE on this surface as well as the different reactivities of intermediate species. Only the stepwise transfer of H atoms, similar to a Horiuti–Polanyi-type mechanism,[37] was considered in this study, which would not favor the preservation of the proton spin correlation in para-hydrogen.

In another DFT study, the reaction thermodynamics of PE and PY hydrogenation on a fully hydroxylated (111) terminated CeO_2 surface were investigated for large H_2/alkyne reactant ratios.[38] The calculations indicated that on this surface, hydrogenation of PY occurs through a low-energy six-membered-ring transition state involving the H–H bond, the adsorbed alkyne, and an adjacent hydroxy group. Whereas this transition state does not result in pairwise addition, as one H atom is transferred to the substrate from H_2 and the other from OH, pairwise addition can occur through a four-membered-ring transition state, even though its activation energy was predicted to be significantly higher on the fully hydroxylated surface.[38] Distinguishing the pairwise and non-pairwise addition pathways is readily achieved by PHIP NMR spectroscopy and is the focus of this paper.

Shaped CeO_2 nanocrystals with surfactant-free surfaces were synthesized by the hydrothermal method[39–41] (see the Supporting Information). Transmission electron micrographs (TEMs) are presented in Figure 1 and in the Supporting Information, Figure S1, and the crystallinity of the nanoparticles was confirmed by X-ray diffraction (XRD; Figure S2). All three shapes feature a cubic fluorite structure.[42,43] The measured Brunauer–Emmett–Teller (BET) surface areas of the nanorods, nanocubes, and nano-octahedra are $60\ m^2 g^{-1}$, $21\ m^2 g^{-1}$, and $4\ m^2 g^{-1}$, respectively. The specific surface areas estimated from the nanocrystal size distributions obtained from an analysis of the TEM images are $71\ m^2 g^{-1}$, $30\ m^2 g^{-1}$, and $2.3\ m^2 g^{-1}$, respectively (see the Supporting Information), in reasonable agreement with the BET surface areas. Reaction rates were normalized to the BET surface area to facilitate comparison of the activities of different surface facets. This approach was established in previous studies of the facet dependence of oxidation and hydrogenation over ceria.[31,35,44] The reactant gases, H_2 (normal or para-enriched) and PE (or PY) were fed into the reactor at flow rates of $600\ mL\,min^{-1}$ and $20\ mL\,min^{-1}$, respectively. The PHIP experiments were performed in ALTADENA[4] mode, where hydrogenation products formed at 5 mT are transported adiabatically to 9.4 T for NMR detection. The setup and reaction conditions are fully described in the Supporting Information and Ref. [19].

In the hydrogenation of PE with 50% para-enriched hydrogen (p-H_2) at temperatures ranging from 150 to 300 °C, all three shapes produced intense ALTADENA-enhanced PA NMR signals (Figures 2 and S3). The signal enhancement and the rate of conversion of PE into PA (Figure 3) were calculated from the fully relaxed, thermally polarized NMR spectra that were acquired on aliquots of reactor effluent (see Figure S4). The 256 signal transients were accumulated using a recycle delay of 5 s.

In agreement with a recent report,[31] we observed superior activity for the nano-octahedra, followed by the nanocubes and then the nanorods at all reaction temperatures. This trend is attributed to the higher density of hydroxy species on the (111) facets (fewer oxygen vacancies).[31] Experimental ALTADENA signal enhancements (per proton) were calculated from the ratios of the hyperpolarized and thermally polarized signals [Eq. (S5)]. The pairwise selectivity was estimated from the ratio of the
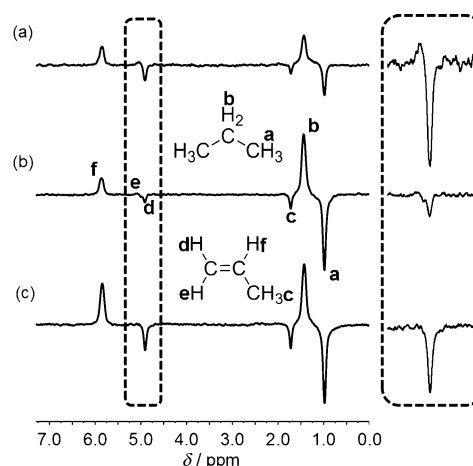
Figure 2. 400 MHz ^{1}H NMR spectra (90° RF pulse flip angle) acquired on the flowing reactor effluent gas resulting from a reactant gas mixture of PE and p-H_2 at a reactor temperature of 375 °C over a) CeO_2 nano-octahedra, b) CeO_2 nanocubes, or c) CeO_2 nanorods. The 32 signal transients were acquired with a 2 s recycle delay. Inset: Expansion of the PE CH_2 (H^d and H^e) spectral region.
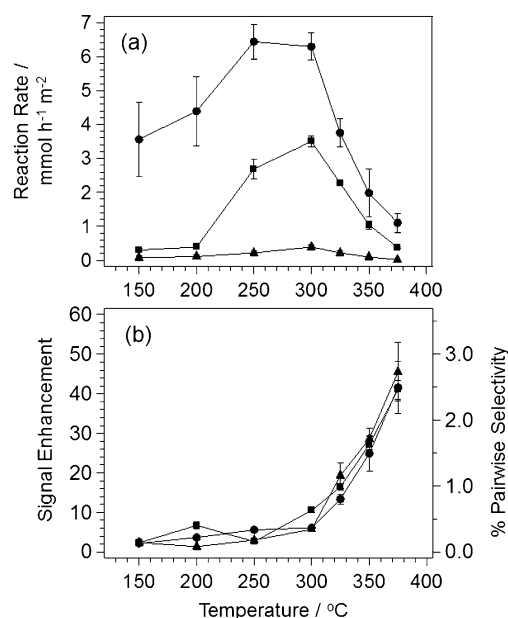
Figure 3. a) Temperature dependence of the rate of PE hydrogenation, calculated from the PA and PE CH_3 peak integrations, normalized to the BET surface areas. b) ALTADENA NMR signal enhancement and pairwise selectivity for the hydrogenation of PE to PA based on the ratio of the ALTADENA and thermally polarized H^a NMR integrals. ●: nano-octahedra; ▲: nanorods; ■: nanocubes.

experimental and theoretical enhancement factors [Eq. (S12)]. The temperature dependence of the signal enhancement and the pairwise selectivity for PE hydrogenation for each catalyst shape is plotted in Figure 3b.

At all temperatures, the enhancement factors for the rods, cubes, and octahedra were found to be the same, within experimental uncertainty. For example, at 375 °C, all shapes yielded an enhancement factor of approximately 40, corresponding to a pairwise selectivity of about 2.4%. This is

comparable to the value observed for PE hydrogenation over supported Pt and Ir catalysts, where hydrogenation occurs mainly by a stepwise (Horiuti–Polanyi) mechanism. Hence, despite substantial differences in the overall catalytic activity, no significant facet dependence of the signal enhancement/pairwise selectivity was observed. The enhancement remained nearly temperature-independent between 150 and 300°C and then increased abruptly from approximately 5 to about 40 at 375°C, indicating that pairwise addition is a thermally activated process. In contrast, the total reaction rate exhibited the opposite trend over the same temperature interval (300–375°C), indicating that pairwise and random addition to the alkene occur through different reaction pathways.

Aside from the PA signal enhancements stemming from pairwise addition to PE, all three CeO₂ shapes also produced intense ALTADENA signals on all protons of PE (Figure 2). These signals are attributed to a pairwise replacement (PR) process, where two protons of the substrate are replaced with two protons from the same para-hydrogen molecule.[19,24] PR-PHIP is akin to signal amplification by reversible exchange (SABRE),[12] in which the para-hydrogen spin order is incorporated into the substrate molecule with no net change in molecular structure. Figure S6 presents the ratios of the H^f multiplet of PE (resulting from PR-PHIP) to the H^a multiplet of PA (resulting from pairwise addition). For all three nanocrystal shapes, the PE/PA signal ratio is seen to increase monotonically with temperature. The signal ratio of approximately 0.7, which was achieved for nanorods and nano-octahedra at 375°C, is approximately three times greater than the highest ratio observed for supported metal nanoparticles.[19]

In the hydrogenation of PY, intense PE ALTADENA signals were also observed for all catalyst shapes. However, no trace of PA formation is evident in the ALTADENA or thermally polarized NMR spectra (Figures 4 and S7). This finding is due to the well-known selectivity of the semi-hydrogenation of PY to PE over CeO₂.[29,31] The spectrum of thermally polarized PE formed by the reaction of PY with normal hydrogen (n-H₂) over cube-shaped ceria nanocrystals at 300°C is shown in Figure 4a. At 300°C and 50% para enrichment, we obtained an enhancement factor of 150 ± 7 based on three independent measurements using the ceria cubes. The enhancement factors for the other two shapes were not determined owing to insufficient signal-to-noise ratios of the thermally polarized PE resonances (because of the smaller surface area of the ceria octahedra and the lower activity of the ceria rods compared with the ceria cubes).

Insights into the mechanism of the pairwise addition to PY and the pairwise replacement in PE could be gleaned from the stereoselectivity of these processes, because the ALTADENA spectrum of PE is sensitive to the stereoselectivity of the addition/replacement.[19] Based on the geometry of the transition state, the concerted addition to PY was predicted to occur in a *syn* fashion.[38] By comparing the experimental spectrum to the spectral simulations for the *cis* and *trans* dispositions of the para-hydrogen spin order (Figure S8), the stereoselectivity could be determined. The experimental spectra obtained for all three shapes (Figures 2 and 4)
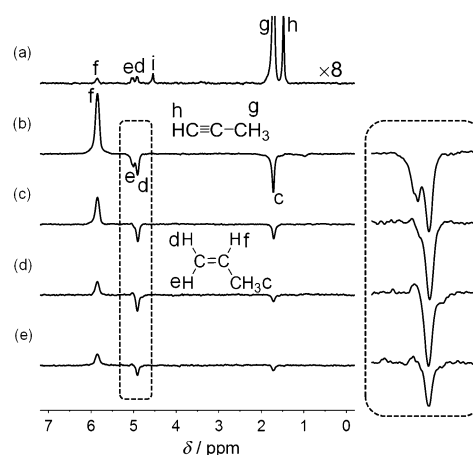
Figure 4. 400 MHz ¹H NMR spectra (90° RF pulse flip angle) of products resulting from PY hydrogenation over shaped ceria nanocrystals. a) Thermally polarized spectrum of the products of hydrogenation over ceria nanocubes with n-H₂ at 300°C. Note the eightfold amplification of the vertical scale relative to the other spectra in this Figure. Peak i was assigned to an alkadiene, as reported previously.[29] b) ALTADENA spectrum (32 scans) resulting from hydrogenation over nanocubes at 300°C using p-H₂. c–e) ALTADENA spectra acquired for the hydrogenation over nanocubes (c), nano-octahedra (d), or nanorods (e) at 375°C with p-H₂. Inset: Expansion of the PE CH₂ (H^d and H^e) region exhibiting *syn* addition stereoselectivity.

indicate *syn* addition to PY and *syn* pairwise replacement in PE. The stereoselectivity of the pairwise replacement process and the temperature dependence of the PE/PA ratio are consistent with the two-step dehydrogenation–rehydrogenation mechanism reported for supported metal nanoparticles.[19]

Calculations of the pairwise selectivity of PY hydrogenation must account for the reduction in the ALTADENA polarization that is due to sharing of the spin order with ancillary protons not originating from H₂. The reduction, which is different for the *cis* and *trans* dispositions of the bilinear spin order, was determined by numerical density operator calculation (see the Supporting Information). Based on an estimated 90% *syn* addition stereoselectivity, the signal enhancement factor on PE at 300°C corresponds to a pairwise selectivity of 2.7 ± 0.1% (see the Supporting Information).

In summary, intense ALTADENA PHIP signals have been observed for the hydrogenation of PE and PY using octahedral, cubic, or rod-shaped CeO₂ nanocrystals. For PY as the reactant, hyperpolarized PE was produced by stereoselective semi-hydrogenation, with no detectable formation of PA. The pairwise selectivities for alkene and alkyne hydrogenation over CeO₂ nanocubes at 300°C are similar. By using 99% para enrichment and eliminating sharing of the para-hydrogen spin order with ancillary spins (e.g., by perdeuteration of PY), we project a signal enhancement of 850 with this catalyst relative to the thermally polarized signal at 298 K and 9.4 T, corresponding to a nuclear spin polarization of approximately 2.7% on the PE CH proton.

The low pairwise selectivity of PY hydrogenation is consistent with the Horiuti–Polanyi mechanism or the DFT-predicted concerted addition involving the PY triple bond,

a hydroxy group, and H_2 in a six-membered ring.[38] The low pairwise selectivity of PE hydrogenation is the same for all three shapes and is similar to that observed on supported metal nanoparticles.[23,27] All shapes were also found to efficiently catalyze pairwise replacement on PE. The *syn* replacement stereoselectivity points to a two-step pairwise replacement process like the one that was reported for supported Pt and Ir catalysts.[19]

We have presented the first investigation of a facet effect on the pairwise selectivity of alkene hydrogenation over a crystalline heterogeneous catalyst. Given that the rate of hydrogenation over ceria is strongly facet-dependent, it seemed plausible that the (100), (110), and (111) surfaces would lead to different pairwise addition selectivities towards PE, but this is not the case. Both random and pairwise addition pathways exhibit the same dependence on the oxygen vacancy density. However, the different temperature dependences for random and pairwise addition are indicative of distinct roles of the oxygen vacancies in these processes. Clearly, para-hydrogen-enhanced NMR spectroscopy can serve as a unique method to explore concerted hydrogenation and pairwise replacement reactions in these catalytic systems.

Acknowledgements

[1] C. R. Bowers, D. P. Weitekamp, *Phys. Rev. Lett.* **1986**, *57*, 2645–2648.
[2] C. R. Bowers, D. P. Weitekamp, *J. Am. Chem. Soc.* **1987**, *109*, 5541–5542.
[3] T. C. Eisenschmid, R. U. Kirss, P. P. Deutsch, S. I. Hommeltoft, R. Eisenberg, J. Bargon, R. G. Lawler, A. L. Balch, *J. Am. Chem. Soc.* **1987**, *109*, 8089–8091.
[4] M. G. Pravica, D. P. Weitekamp, *Chem. Phys. Lett.* **1988**, *145*, 255–258.
[5] R. Eisenberg, *Acc. Chem. Res.* **1991**, *24*, 110–116.
[6] C. R. Bowers in *Encyclopedia of Nuclear Magnetic Resonance*, Vol. 9 (Eds.: D. M. Grant, R. K. Harris), Wiley, Chichester, **2002**, p. 750.
[7] S. K. Hasnip, S. B. Duckett, C. J. Sleigh, D. R. Taylor, G. K. Barlow, M. J. Taylor, *Chem. Commun.* **1999**, 1717–1718.
[8] D. Blazina, S. B. Duckett, J. P. Dunne, C. Godard, *Dalton Trans.* **2004**, 2601–2609.
[9] J. P. Dunne, D. Blazina, S. Aiken, H. A. Carteret, S. B. Duckett, J. A. Jones, R. Poli, A. C. Whitwood, *Dalton Trans.* **2004**, 3616–3628.
[10] A. M. Balu, S. B. Duckett, R. Luque, *Dalton Trans.* **2009**, 5074–5076.
[11] L.-S. Bouchard, S. R. Burt, M. S. Anwar, K. V. Kovtunov, I. V. Koptyug, A. Pines, *Science* **2008**, *319*, 442–445.
[12] R. W. Adams, J. A. Aguilar, K. D. Atkinson, M. J. Cowley, P. I. P. Elliott, S. B. Duckett, G. G. R. Green, I. G. Khazal, J. Lopez-Serrano, D. C. Williamson, *Science* **2009**, *323*, 1708–1711.
[13] K. V. Kovtunov, V. V. Zhivonitko, A. Corma, I. V. Koptyug, *J. Phys. Chem. Lett.* **2010**, *1*, 1705–1708.
[14] I. V. Skovpin, V. V. Zhivonitko, R. Kaptein, I. V. Koptyug, *Appl. Magn. Reson.* **2013**, *44*, 289–300.
[15] B. J. A. van Weerdenburg, S. Gloggler, N. Eshuis, A. H. J. Engwerda, J. M. M. Smits, R. de Gelder, S. Appelt, S. S. Wymenga, M. Tessari, M. C. Feiters, B. Blumich, F. P. J. T. Rutjes, *Chem. Commun.* **2013**, *49*, 7388–7390.
[16] F. Shi, A. M. Coffey, K. W. Waddell, E. Y. Chekmenev, B. M. Goodson, *Angew. Chem. Int. Ed.* **2014**, *53*, 7495–7498; *Angew. Chem.* **2014**, *126*, 7625–7628.
[17] N. Eshuis, N. Hermkens, B. J. A. van Weerdenburg, M. C. Feiters, F. P. J. T. Rutjes, S. S. Wijmenga, M. Tessari, *J. Am. Chem. Soc.* **2014**, *136*, 2695–2698.
[18] S. Glöggler, A. M. Grunfeld, Y. N. Ertas, J. McCormick, S. Wagner, P. P. M. Schleker, L.-S. Bouchard, *Angew. Chem. Int. Ed.* **2015**, *54*, 2452–2456; *Angew. Chem.* **2015**, *127*, 2482–2486.
[19] R. Zhou, E. W. Zhao, W. Cheng, L. M. Neal, H. Zheng, R. E. Quiñones, H. E. Hagelin-Weaver, C. R. Bowers, *J. Am. Chem. Soc.* **2015**, *137*, 1938–1946.
[20] K. V. Kovtunov, I. E. Beck, V. I. Bukhtiyarov, I. V. Koptyug, *Angew. Chem. Int. Ed.* **2008**, *47*, 1492–1495; *Angew. Chem.* **2008**, *120*, 1514–1517.
[21] V. V. Zhivonitko, K. V. Kovtunov, I. E. Beck, A. B. Ayupov, V. I. Bukhtiyarov, I. V. Koptyug, *J. Phys. Chem. C* **2011**, *115*, 13386–13391.
[22] O. G. Salnikov, K. V. Kovtunov, D. A. Barskiy, V. I. Bukhtiyarov, R. Kaptein, I. V. Koptyug, *Appl. Magn. Reson.* **2013**, *44*, 279–288.
[23] K. V. Kovtunov, V. V. Zhivonitko, I. V. Skovpin, D. A. Barskiy, I. V. Koptyug, *Top. Curr. Chem.* **2013**, *338*, 123–180.
[24] K. V. Kovtunov, V. V. Zhivonitko, I. V. Skovpin, D. A. Barskiy, O. G. Salnikov, I. V. Koptyug, *J. Phys. Chem. C* **2013**, *117*, 22887–22893.
[25] K. V. Kovtunov, D. A. Barskiy, O. G. Salnikov, A. K. Khudorozhkov, V. I. Bukhtiyarov, I. P. Prosvirin, I. V. Koptyug, *Chem. Commun.* **2014**, *50*, 875–878.
[26] A. Corma, O. G. Salnikov, D. A. Barskiy, K. V. Kovtunov, I. V. Koptyug, *Chem. Eur. J.* **2015**, *21*, 7012–7015.
[27] D. A. Barskiy, O. G. Salnikov, K. V. Kovtunov, I. V. Koptyug, *J. Phys. Chem. A* **2015**, *119*, 996–1006.
[28] A. Trovarelli, *Catalysis by ceria and related materials*, Imperial College Press, London, **2002**.
[29] G. Vilé, B. Bridier, J. Wichert, J. Pérez-Ramírez, *Angew. Chem. Int. Ed.* **2012**, *51*, 8620–8623; *Angew. Chem.* **2012**, *124*, 8748–8751.
[30] C. W. Sun, H. Li, L. Q. Chen, *Energy Environ. Sci.* **2012**, *5*, 8475–8505.
[31] G. Vilé, S. Colussi, F. Krumeich, A. Trovarelli, J. Pérez-Ramírez, *Angew. Chem. Int. Ed.* **2014**, *53*, 12069–12072; *Angew. Chem.* **2014**, *126*, 12265–12268.
[32] N. C. Nelson, J. S. Manzano, A. D. Sadow, S. H. Overbury, I. I. Slowing, *ACS Catal.* **2015**, *5*, 2051–2061.
[33] J. Carrasco, G. Vile, D. Fernandez-Torre, R. Perez, J. Perez-Ramirez, M. V. Ganduglia-Pirovano, *J. Phys. Chem. C* **2014**, *118*, 5352–5360.

[34] D. A. Barskiy, K. V. Kovtunov, A. Primo, A. Corma, R. Kaptein, I. V. Koptyug, *ChemCatChem* **2012**, *4*, 2031 – 2035.

[35] M. Li, Z. Wu, S. H. Overbury, *J. Catal.* **2013**, *306*, 164 – 176.

[36] Tana, M. L. Zhang, J. Li, H. J. Li, Y. Li, W. J. Shen, *Catal. Today* **2009**, *148*, 179 – 183.

[37] I. Horiuti, M. Polanyi, *Trans. Faraday Soc.* **1934**, *30*, 1164 – 1172.

[38] M. García-Melchor, L. Bellarosa, N. López, *ACS Catal.* **2014**, *4*, 4015 – 4020.

[39] Z. Wu, M. Li, J. Howe, H. M. Meyer, S. H. Overbury, *Langmuir* **2010**, *26*, 16595 – 16606.

[40] H.-X. Mai, L.-D. Sun, Y.-W. Zhang, R. Si, W. Feng, H.-P. Zhang, H.-C. Liu, C.-H. Yan, *J. Phys. Chem. B* **2005**, *109*, 24380 – 24385.

[41] W. Huang, Y. Gao, *Catal. Sci. Technol.* **2014**, *4*, 3772 – 3784.

[42] F. Esch, S. Fabris, L. Zhou, T. Montini, C. Africh, P. Fornasiero, G. Comelli, R. Rosei, *Science* **2005**, *309*, 752 – 755.

[43] J. Conesa, *Surf. Sci.* **1995**, *339*, 337 – 352.

[44] Z. Wu, M. Li, S. H. Overbury, *J. Catal.* **2012**, *285*, 61 – 73.